SMC-TR-04-22

AEROSPACE REPORT NO.
TR-2004(8570)-5

The Energetic Electron Response to Magnetic Storms: HEO Satellite Observations

10 July 2004

Prepared by

J. F. FENNELL,[1] J. B. BLAKE,[1] R. FRIEDEL,[2]
and S. KANEKAL[3]

[1]Space Science Applications Laboratory
Laboratory Operations
[2]Los Alamos National Laboratory, Los Alamos, NM 87545
[3]Catholic University, Washington D. C. 20064

Prepared for

SPACE AND MISSILE SYSTEMS CENTER
AIR FORCE SPACE COMMAND
2430 E. El Segundo Boulevard
Los Angeles Air Force Base, CA 90245

Engineering and Technology Group

THE AEROSPACE CORPORATION
EL SEGUNDO, CALIFORNIA

This report was submitted by The Aerospace Corporation, El Segundo, CA 90245-4691, under Contract No. FA8802-04-C-0001 with the Space and Missile Systems Center, 2430 E. El Segundo Blvd., Los Angeles Air Force Base, CA 90245. It was reviewed and approved for The Aerospace Corporation by J. A. Hackwell, Principal Director, Space Science Applications Laboratory. Michael Zambrana was the project officer for the Mission-Oriented Investigation and Experimentation (MOIE) program.

This report has been reviewed by the Public Affairs Office (PAS) and is releasable to the National Technical Information Service (NTIS). At NTIS, it will be available to the general public, including foreign nationals.

This technical report has been reviewed and is approved for publication. Publication of this report does not constitute Air Force approval of the report's findings or conclusions. It is published only for the exchange and stimulation of ideas.

Michael Zambrana
SMC/AXE

REPORT DOCUMENTATION PAGE

Form Approved
OMB No. 0704-0188

1. REPORT DATE (*DD-MM-YYYY*)	2. REPORT TYPE	3. DATES COVERED *(From - To)*
10-07-2004		

4. TITLE AND SUBTITLE

The Energetic Electron Response to Magnetic Storms: HEO Satellite Observations

5a. CONTRACT NUMBER
FA8802-04-C-0001

5b. GRANT NUMBER

5c. PROGRAM ELEMENT NUMBER

6. AUTHOR(S)

J. F. Fennell, J. B. Blake, R. Friedel, and S. Kanekal

5d. PROJECT NUMBER

5e. TASK NUMBER

5f. WORK UNIT NUMBER

7. PERFORMING ORGANIZATION NAME(S) AND ADDRESS(ES)

The Aerospace Corporation
Laboratory Operations
El Segundo, CA 90245-4691

8. PERFORMING ORGANIZATION REPORT NUMBER

TR-2004(8570)-5

9. SPONSORING / MONITORING AGENCY NAME(S) AND ADDRESS(ES)

Space and Missile Systems Center
Air Force Space Command
2450 E. El Segundo Blvd.
Los Angeles Air Force Base, CA 90245

10. SPONSOR/MONITOR'S ACRONYM(S)
SMC

11. SPONSOR/MONITOR'S REPORT NUMBER(S)
SMC-TR-04-22

12. DISTRIBUTION/AVAILABILITY STATEMENT

Approved for public release; distribution unlimited.

13. SUPPLEMENTARY NOTES

14. ABSTRACT

The energetic electron observations from the HEO 97-068 satellite are used to study the electron response to magnetic storms in the inner magnetosphere during 1998–2002. The observations cover L values in the range $2.5 \leq L \leq 6$. The same L values are covered at both high (>2.3 Re) and low (<1.2 Re) geocentric altitudes. The electron flux histories at low and high altitudes are directly compared and are found to track with a high degree of fidelity independent of flux levels and energy for a wide range of L values. The low-altitude >1.5 MeV electron fluxes were ~10–16% of the high-altitude fluxes for L = 3–5.5, except during the rapid post-storm flux rises. The decay of the post-storm electron fluxes were examined to obtain the e-folding decay times at L = 3, near the peak of the outer zone. The high-altitude >1.5 MeV electron fluxes were found to have three distinct 1/e decay times of about 5, 10.5, and 17.5 days. The 5 and 10.5 day e-folding times ocurred in the first several days after the post-storm fluxes peaked during 2000–2001 and 1998 periods, respectively. The longer e-folding times occurred late in the decay history. These results support the view that the acceleration and loss mechanisms are operating essentially simultaneously over much of the outer zone.

15. SUBJECT TERMS

Trapped radiation, Magnetic storms

16. SECURITY CLASSIFICATION OF:			17. LIMITATION OF ABSTRACT	18. NUMBER OF PAGES	19a. NAME OF RESPONSIBLE PERSON
					Joseph Fennell
a. REPORT	b. ABSTRACT	c. THIS PAGE			19b. TELEPHONE NUMBER *(include area code)*
UNCLASSIFIED	UNCLASSIFIED	UNCLASSIFIED		16	(310)336-7075

Acknowledgments

Work at Aerospace was supported by The Aerospace Corporation MOIE program (via U.S. Air Force under Contract No. FA8802-04-C-0001) and NASA grant NAG5-10972. The work at Los Alamos was supported by NASA LWS grant W-19957 and DOE OBES. The work at Catholic U. was supported by NASA analysis funding for SAMPEX and Polar Ceppad Global Geospace investigations. JFF thanks T. P. O'Brien, J. Roeder, and K. Lorentzen for useful discussions.

Contents

1. Introduction 1

2. Instrumentation and Data 3

3. Observations 5

   3.1 High/Low-Altitude Flux Comparisons 7

   3.2 Electron Decays at L = 3 10

4. Discussion 14

References 17

Figures

1. Daily average >1.5 MeV electron intensity for several L values during the period April 1998 to April 1999 (upper panels) and the estimated plasmapause position ($L_{PP;}$ black line) and the range of L where microbursts ($L_{Microbursts}$; blue and red markings) were observed by SAMPEX (bottom panel) 6

2. Plot of high (black) and low (red) Ee>1.5 MeV fluxes at L = 3 7

3. Ratio of four years of low to high altitude Ee>1.5 MeV electron fluxes from HEO 97-068 for several different L values. 8

4. HEO 97-068 perigee altitude history 9

5. Comparison of low and high altitude HEO3 fluxes and their ratio at L = 3 for the interval around the 22 Sept 1999 magnetic storm. 9

6. Ratio of four years of low to high altitude electron fluxes from HEO 97-068 L = 4 for several energies. 9

7. Electron flux decay at three energies following the May 1998 magnetic storm 11

8. Flux history of electrons >1.5 MeV at L = 3. 12

9. Histogram of e-folding decay times, in days, for the data in Figure 8 13

Table

1. Statistics for Ratios of Low/High-Altitude Fluxes 10

1. Introduction

Blake et al. (1997) used orbit integrated HEO dose data to infer that the combination of a high-speed solar wind stream (HSS) in conjunction with a southward turning of the interplanetary magnetic field (IMF) was key to enhancement in the radiation belt fluxes. They used isolated HSS events in their study to simplify the relationships. They showed that a northward IMF turning negated the HSS and that losses can occur without subsequent flux enhancements. Recent work by Knekal et al. (2001; 1999) has shown that low-altitude polar orbiting satellites such as SAMPEX can readily track the rsponses of the electron radiation to magnetic storms in the inner magnetosphere and that the high-altitude and low-altitude fluxes track each other closely. Kanekal et al. (2001) used Polar, HEO, and SAMPEX satellite data to show that the fluxes measured at high and low altitudes tracked well most of the time. They used superposed epoch analyses to show that the delays between flux changes at Polar and SAMPEX were consistent with zero lag. The daily HEO dose at two energies (>1.5 and 3.5 MeV) and fluxes from the SAMPEX 2–6 MeV channel were integrated over the $2.5 \leq L \leq 6.5$ for comparison. While that comparison showed a strong similarity in time history at both HEO and SAMPEX, the different instrument energy responses did not allow for as detailed an intercomparison as was done for the Polar and SAMPEX data. Thus, no previous analyses have compared high- and low-altitude fluxes using the same set of instrumentation. That is one of the main features of this report.

This page intentionally blank.

2. Instrumentation and Data

This study uses data taken by a high Earth orbiting, HEO, satellite in a ~1.15 x 7.2 R_E orbit inclined at ~63° with a ~12-h period. The satellite is designated HEO 1997-086 (or HEO3). HEO3 covers a wide range of L values at both mid to high altitudes and at low altitude. The perigee of HEO3 varied between 1.18 and 1.33 Re geocentric (see Figure 4) during the 1998-2002 period.

The data were obtained using five integral energy sensors that measured electrons with energies >0.23, >0.45, >0.6, >1.5, and >2.9 MeV. The four highest energy sensors make omnidirectional flux measurements. The >0.23 MeV electron data are from a proton-electron telescope with a ~15° conical field of view (Blake et al. 1997). For much of this study, we emphasize the results from the >1.5 MeV electrons because most of the recent results in the literature concerning electron acceleration and transport in the inner magnetosphere have emphasized MeV electrons.

We focus on electron data taken during the 1998–2002 period for this report. This includes most of the stormtime events that were highlighted during the Physics and Modeling of the Inner Magnetosphere conference held in Helsinki, FI. We examine the energetic electron storm responses from two perspectives: (1) the tracking of high- and low-altitude electron fluxes using the same instrumentation; and (2) the post-storm decay of the fluxes at L = 3, inside the nominal plasmasphere.

This page intentionally blank.

3. Observations

First, we examine the flux variability taken at high altitudes (>2.5 Re geocentric) for several L values. The top panels in Figure 1 show the daily average >1.5 MeV electron flux history during the April 1998 through March 1999 period at L = 2.5–4. The bottom panel shows a line plot of the estimated minimum daily plasmapause position [*O'Brien and Moldwin,* 2003]. Superimposed on the line plot are colored bars indicating where electron precipitation microbursts [*Lorentzen et al.*, 2001a and 2001b; *O'Brien et al.*, 2003] were observed at $L \leq 4$ (red bars) and $L \geq 4$ (blue bars).

The data in Figure 1 are plotted as line plots instead of in L versus time spectrogram form so that differences from one L value to the next clearly stand out. Figure 1 shows that the electron fluxes are most variable at large L values with sharp sudden flux drops for short intervals of time. This variability is even greater for $L > 4$ (not shown). The sharp flux drops correspond with periods of magnetic activity, in many cases storm related.

At the lowest L values, one observes sudden electron flux enhancements followed by decay. At L = 2.5, the flux enhancements rise out of the instrument background and are observed only for the storms labeled by the months in which they occurred. At L = 4, there is a series of flux enhancements, most of which are preceded by sharp flux drops as noted above. At the bottom of the panels for each L, we have indicated the occurrence of precipitation microbursts, observed by SAMPEX, as red marks. The thickness of the red marks represents the duration of microburst occurrence for $L \leq 4$. There is a strong association of the flux dropouts and subsequent rapid increases with the appearance of the microbursts. All microbursts caused a flux decrease, but not all such decreases were followed by flux enhancements. It is clear that combining such data from SAMPEX, at low altitude, with the HEO data, at high altitude, highlights features of the electron acceleration and loss processes that cannot be garnered from either dataset in isolation. These and other microburst associations are discussed, in detail, in a paper by O'Brien et al. [2003] and will not be expanded upon here.

Only the strongest storms caused flux enhancements in the electron slot region ($2 < L < 3$). Storms that caused slot region fillings are also associated with strong erosion of the plasmasphere, as shown at the bottom of Figure 1. Each time Dst was <–150 (not shown) and the plasmapause was estimated to be below L = 3, the electron fluxes in the slot showed an increase. This indicates that erosion of the plasmapause to low L is one process that occurs simultaneously with electrons being transported to or accelerated at equally low L. It is not clear from the observations in Figure 1 whether the erosion of the plasmapause is a necessary condition for all low-L electron flux enhancements. Shock acceleration of the type that occurred during the famous March 1991 event [*Li et al.*, 1993; *Blake et al.*, 1992] may occur without plasmapause erosion. However, the relationship between plasmapause erosion and low-L electron enhancements needs to be examined in detail. The IMAGE FUV measurements combined with HEO and SAMPEX data could be used to perform such a study.

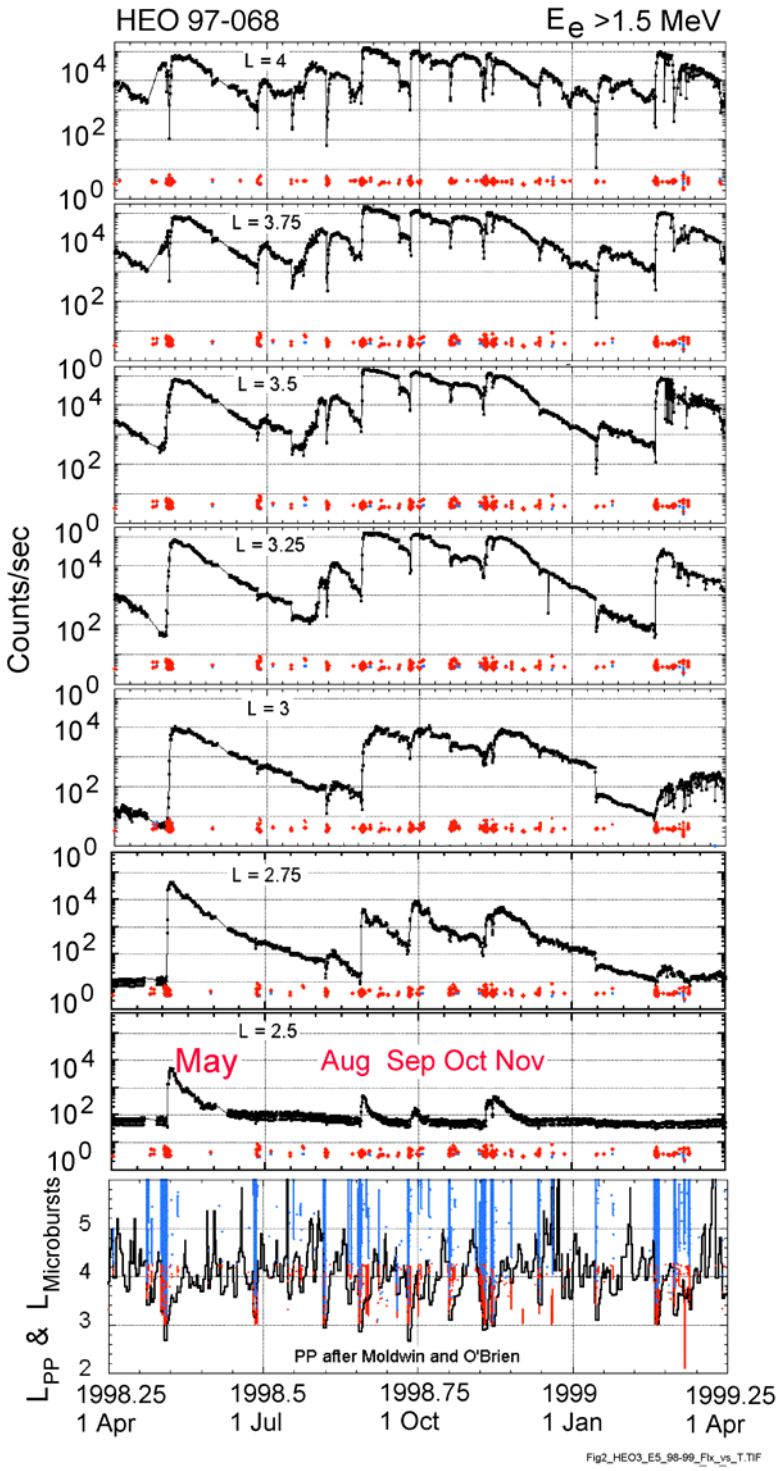

Figure 1. Daily average >1.5 MeV electron intensity for several L values during the period April 1998 to April 1999 (upper panels) and the estimated plasmapause position ($L_{PP;}$ black line) and the range of L where microbursts ($L_{Microbursts}$; blue and red markings) were observed by SAMPEX (bottom panel)

3.1 High/Low-Altitude Flux Comparisons

This preliminary study takes advantage of the fact that the same sensors measure electron fluxes at both high and low altitudes at the same L values because of the highly elliptical orbit of HEO3. This allows us to compare the electron fluxes at different altitudes without worrying about whether the sensor responses are the same.

To show the relationship between the high-altitude and low-altitude electron fluxes, we first look to Figure 2 where the time history of low (red) and high (black) altitude Ee > 1.5 MeV electron intensities at L = 3 are shown for the 1998–2002 period. This plot shows that the electron fluxes varied over several orders of magnitude at both high and low altitudes and that the fluxes at the two altitudes appear to track very well.

This tracking of the high- and low-altitude fluxes is further demonstrated in Figure 3, which shows the ratio of the low-altitude to high-altitude fluxes for multiple L values. Several features are evident in Figure 3. The most striking feature occurs at the highest L values where an annual variation is observed in the ratio. The annual variation results from the fact that we used the IGRF field model for this initial study, and it does not contain the day-night asymmetries of the real field that are most prominent at large L, high latitudes, and large distances from Earth. The HEO3 database we are using already has all the data in B-L coordinates based on the IGRF and was considered sufficient for this initial low/high-altitude comparison. More complicated field models could be used in the future, if warranted. However, no field model does a good job of representing the real field asymmetries at HEO altitudes and latitudes, especially during magnetic storms. The best of the models are compute intensive and not easily applicable to large datasets like the HEO datasets. We have tried the Olson-Pfitzer [*Olson, et al.,* 1979], T87 and T96 [*Tsyganenko,* 1995; 1996 and refs. therein] models for limited periods and found that these models often predicted that HEO3 was on open field lines when the data clearly indicated it was not and vice versa, especially during disturbed periods.

In any case, the peaks in the ratio at large L at the same season from year to year indicates the constancy of the low/high-altitude flux ratio. Figure 3 shows that at L ≤ 4.5, the flux ratios are relatively constant independent of the variation in flux levels seen in Figures 1 and 2. The smallest L values show a general rise in the flux ratio from 1998 to 2001 and a decline after that. This variation

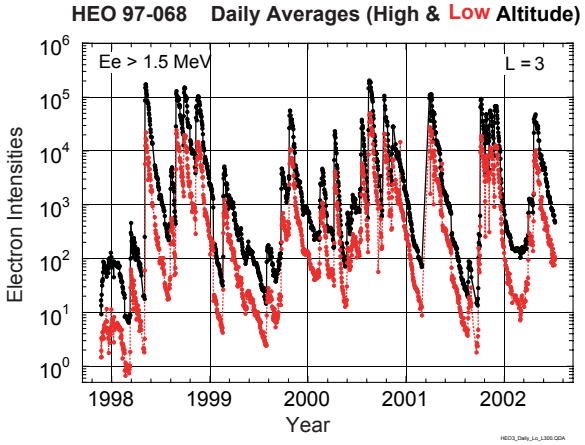

Figure 2. Plot of high (black) and low (red) Ee>1.5 MeV fluxes at L=3.

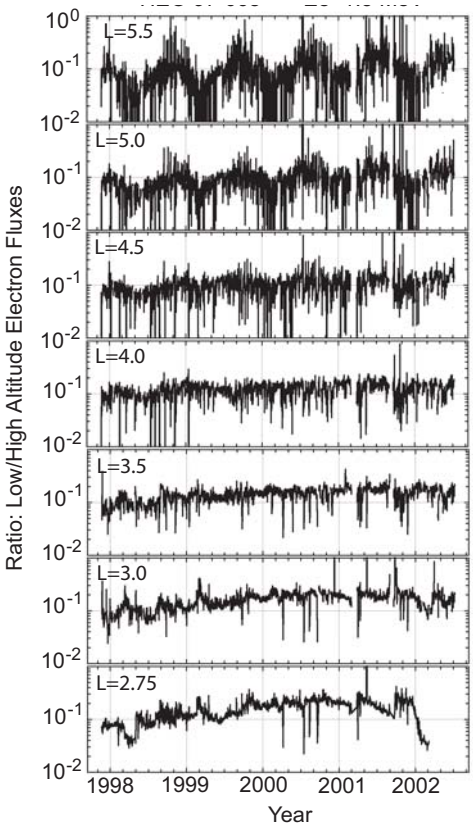

Figure 3. Ratio of four years of low to high altitude Ee>1.5 MeV electron fluxes from HEO 97-068 for several different L values.

resulted from the changing perigee altitude of HEO3 with time, as shown in Figure 4. This change in the altitude of the low-altitude flux measurement has a greater effect at small L values than large ones because the resultant ratio B_{low}/B_{high} changes most dramatically for the smallest L's.

The other major feature observed in Figure 3 are sharp, short-duration decreases in the ratios. These decreases mostly occur at the time of large flux increases. They are consistent with the high-altitude fluxes increasing faster than those at low altitudes at the same L. Figure 5 shows an expanded example of one of these downward ratio spikes from the flux increase that occurred in conjunction with a magnetic storm on 22 Sept 1999. The plot shows that the short-term decrease in the ratio was associated with the difference in the rate of flux increase (here at L = 3) at low and high altitudes. The ratio returned to its nominal pre-storm value as the fluxes reached their maximum values and started to decay.

Figure 6 shows that the low/high-altitude flux ratios at L = 4 are relatively constant for electrons with energies from >0.23 to >2.9 MeV. This is also true for other L values (not shown). Figure 6 indicates that the processes that maintain these low/high-altitude electron flux ratios are not strongly energy dependent at least over the energy range measured.

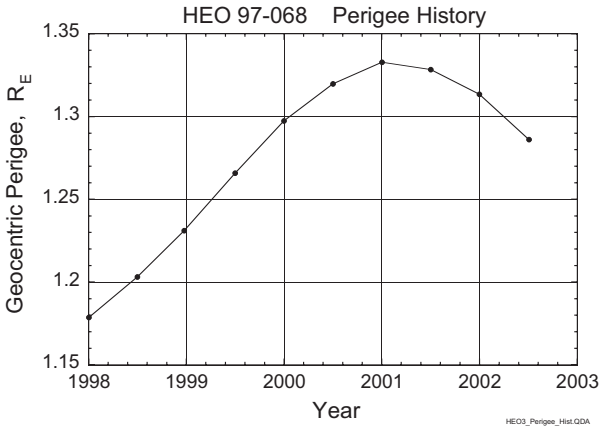

Figure 4. HEO 97-068 perigee altitude history.

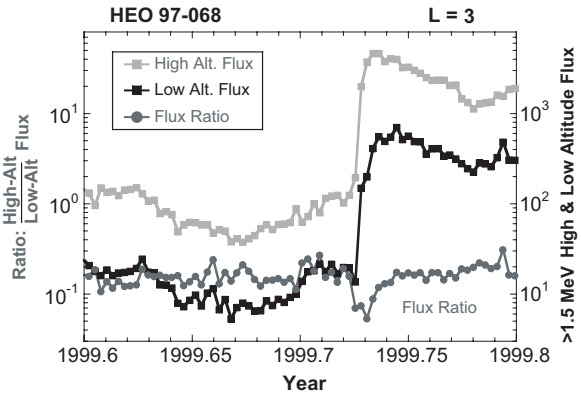

Figure 5. Comparison of low and high altitude HEO3 fluxes and their ratio at L = 3 for the interval around the 22 Sept. 1999 magnetic storm.

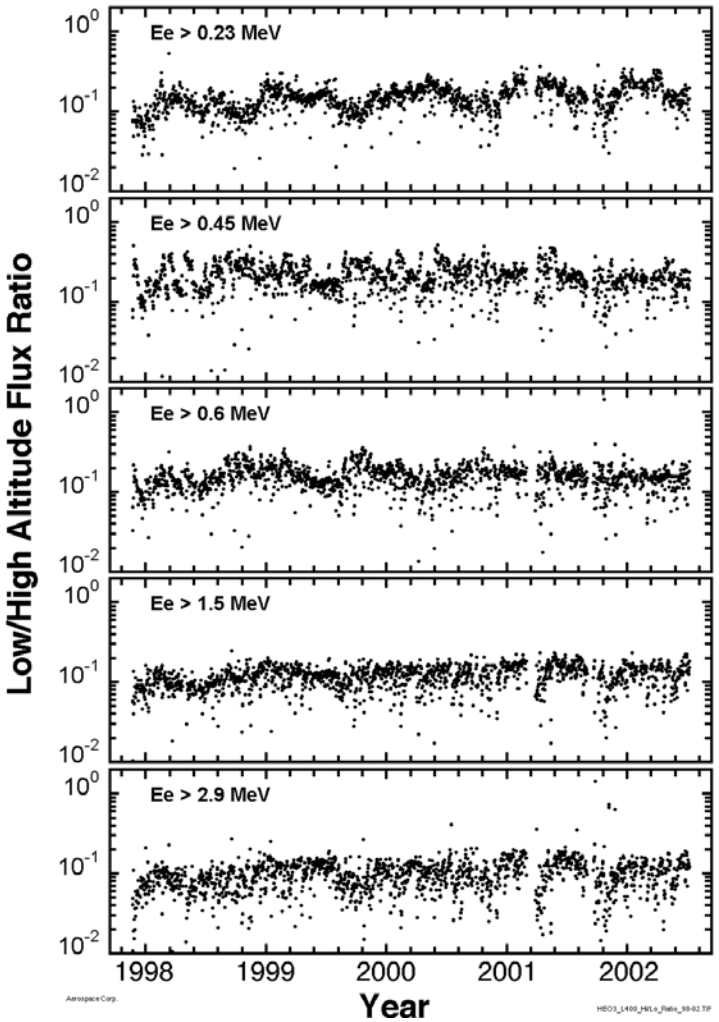

Figure 6. Ratio of four years of low to high altitude electron fluxes from HEO 97-068 L = 4 for several energies.

Table 1 shows the statistics for the distributions of >1.5 MeV flux ratios at six different L values. The statistics were obtained from the data shown in Figure 3. The plots of the distributions (not shown) had relatively narrow peaks and the majority were symmetric about the mean. This is evidenced by the fact that the mean and median values are nearly the same. As the table shows, the mean of the low/high-altitude flux ratios were in the range of 0.09 to 0.16 for L = 3–5.5, with the ratio decreasing with increasing L. Thus, the high-altitude fluxes were roughly a factor of 6 to 11 higher than those at low altitude.

Figures 1–3 along with Table 1 emphasize the fact that, independent of the absolute flux levels, the magnetospheric processes that redistribute electrons radially and along the field lines do so efficiently and globally except for short intervals during the episodic rapid flux increases associated with magnetic storms (as shown in Figure 5).

Table 1. Statistics for Ratios of Low/High-Altitude Fluxes

L	No. Points	Mean	Median	Std. Dev.
3.0	1555	0.159	0.162	0.053
3.5	1559	0.140	0.143	0.043
4.0	1559	0.120	0.121	0.040
4.5	1502	0.100	0.099	0.041
5.0	1507	0.091	0.085	0.049
5.5	1494	0.096	0.082	0.069

3.2 Electron Decays at L = 3

At the lower L values, where flux dropouts are rare, the losses are thought to be controlled by coulomb losses (dE/dx losses) and pitch angle scattering of the electrons by interactions with the plasmaspheric Hiss. As Figure 1 shows, the plasmasphere boundary rarely reached L = 3 and then only during storm main and early recovery phases. Thus, we expect the loss rates at $L \leq 3$ to be consistent. With this in mind, we examined the electron decay rates at L = 3 to see how they may relate to the near constancy of the low/high-altitude flux ratios noted above. Figure 7 sets the stage for this part of the study. It shows the flux rise and subsequent decay following the May 1998 magnetic storm. This storm had a minimum D_{ST} of –205 nT. Figure 7 also shows where SAMPEX observed precipitation microbursts. The microbursts were intense and occurred primarily just before and during the post storm flux increases at all energies.

An exponential fit to the flux decay was made for each energy shown in Figure 7. The Ee >0.6 and >1.5 MeV data could not be fit with a single e-folding value over the full period shown so the period beyond day 40 (9 June 1998) was fit separately. This change in the decay rate late in the decay period is a common feature in the HEO3 data.

Figure 7 is an example of the way L = 3 electron decay data was gathered for the >1.5 MeV electron fluxes for events that occurred between 1 January 1998 and 1 July 2001. Twenty clear electron flux enhancements occurred at L = 3 during this period, as shown in Figure 8. The intervals from a few days after the flux peaked to the next enhancement were piecewise fit to represent the decay history. In Figure 8, the early part of the decay is flagged in blue, and the later part in red and/or green where

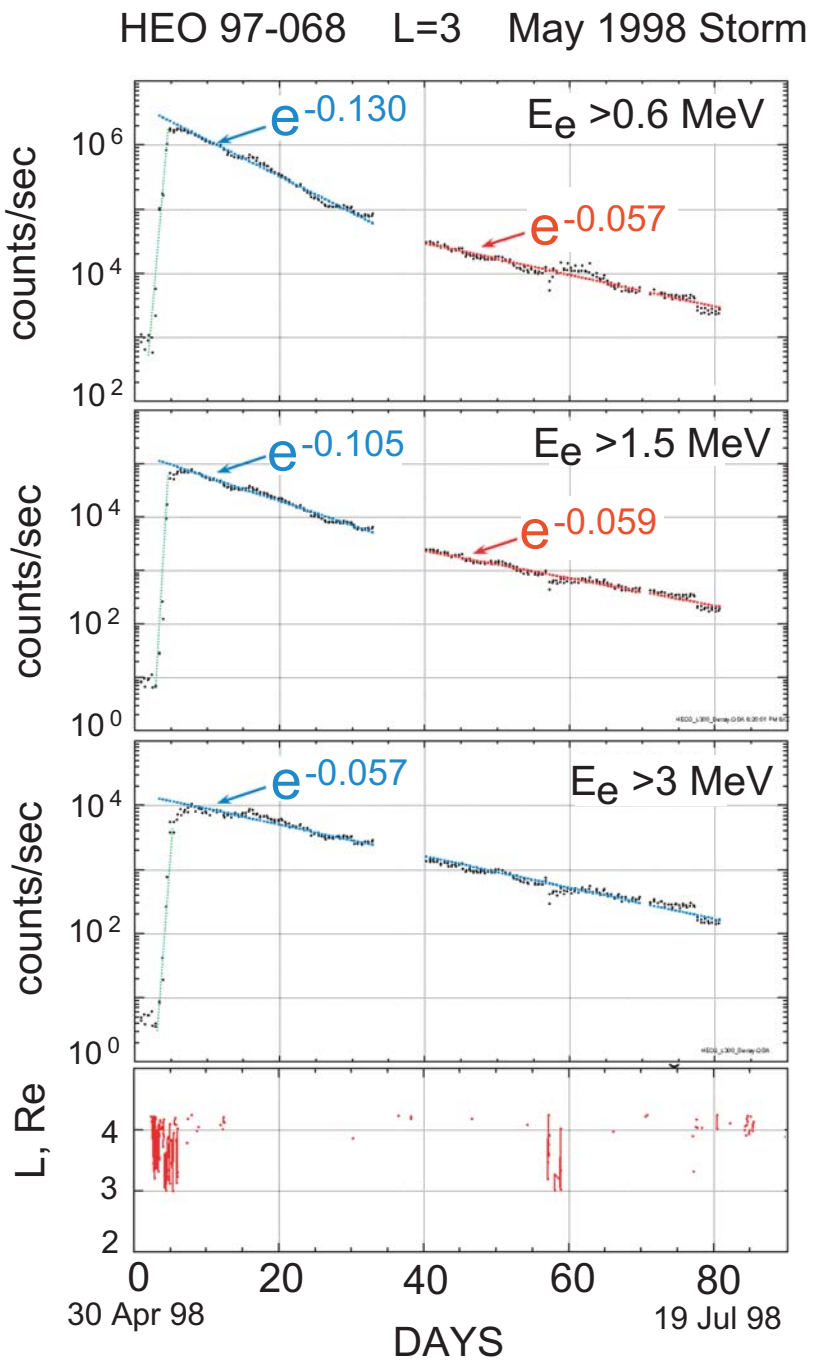

Figure 7. Electron flux decay at three energies following the May 1998 magnetic storm. The bottom panel shows where SAMPEX observed precipitation microbursts.

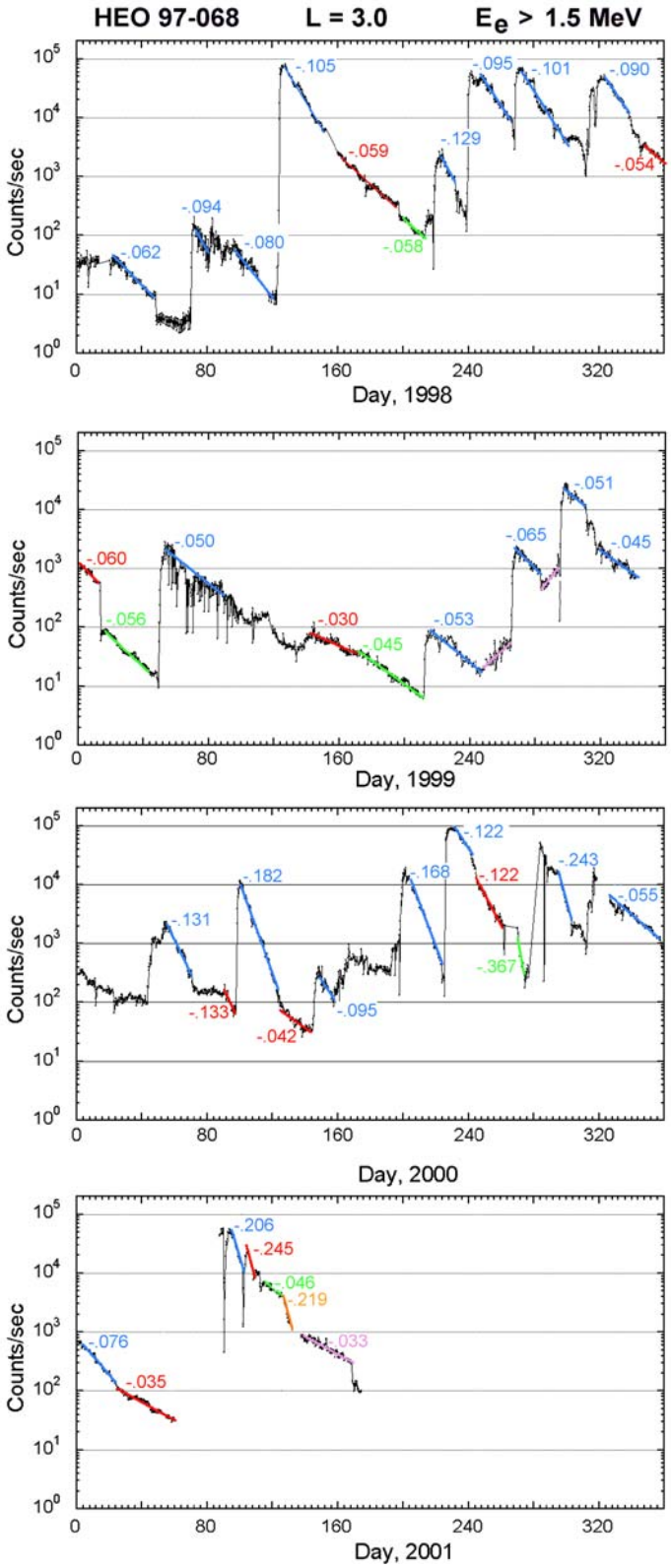

Figure 8. Flux history of electrons >1.5 MeV at L = 3.

a single fit could not represent the decay. There were intervals where magnetic activity caused sudden drops in the electron flux. These were usually followed by a continuation of the decay with 1/e times somewhat longer than the early decays. These are flagged in red or green and treated as late decay intervals.

The e-folding decay times derived from Figure 8 are plotted in histogram form in Figure 9. The set of e-folding times clustered around three distinct periods: 5, 10.5 and 17.5 days. The error bars are based on a multi-variant error analysis [*Evans et al.*, 2000]. The mean 1/e decay time for all intervals was ~14 days. The enhanced electron fluxes caused by the large storms in May, Sept, Oct, and Nov. 1998 had early 1/e decay periods of 9.5–10.5 days, which is very similar to the results obtained with SAMPEX by Baker et al. [1994] and consistent with past theoretical modeling [*Lyons and Thorne*, 1973]. The shortest early 1/e decay periods of ~5 days occurred following the flux enhancements in 2000 and 2001. All the secondary or late decay intervals had decay periods longer than the early decays and were more variable. These contributed to the broad peak near 17.5 days in Figure 9.

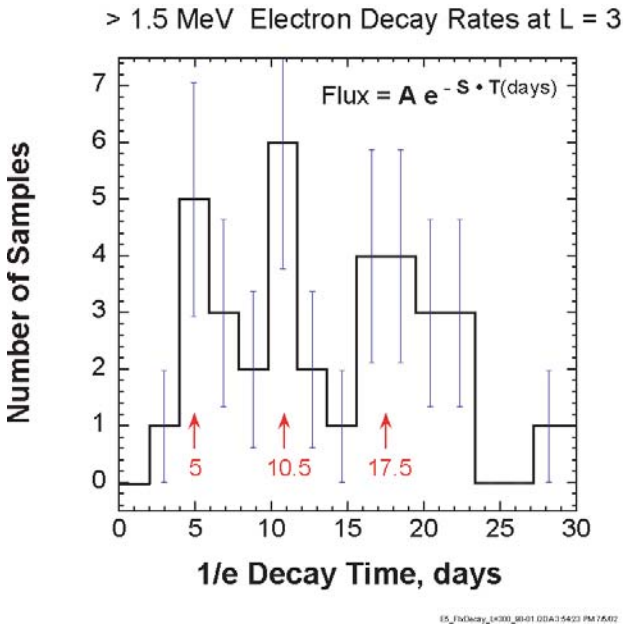

Figure 9. Histogram of e-folding decay times, in days, for the data in Figure 8.

This page intentionally blank.

4. Discussion

The low/high-altitude flux ratio results obtained using the HEO3 data complement and reinforce the results obtained by Kanekal et al [1999, 2001] using SAMPEX and Polar data. The fact that the HEO3 ratios were obtained with a single set of instrumentation removes all doubt that the close tracking of the fluxes at low and high altitudes are real. With the HEO3 data, we have shown that the fluxes at the different altitudes are related by a nearly constant multiplier independent of energy and L over a significant range of L values. This means that low-altitude satellites could be used to monitor the electron radiation belt fluxes at high altitudes, even near the equator, with a reasonable degree of accuracy. One only needs to determine the scaling factors (i.e., flux ratios) between the flux measured at the magnetic equator and at a low-altitude platform. Then the observations obtained by a low-altitude platform, with its high repeat rate for traversals through a wide range of L values, could be used to represent the time-dependent state of the radiation belts. We would suggest that such a platform be somewhat higher than SAMPEX, which spends significant time in both the drift and bounce loss regions. However, it need not be much higher. One to two thousand kilometer altitude circular polar would be a reasonable orbit.

These results show that the processes transporting relativistic electrons from near the equator to low altitudes do so in a manner that keeps the low/high-altitude flux ratios constant on time scales of the order of one to a few days, even during periods of extreme flux changes. What we cannot tell from the current study is how these processes work to maintain the flux ratios. Part of the answer lies in the flux decays. The decay times indicate that combined transport and loss process along the field lines matches expectations for wave-particle interaction models of the type discussed by Lyons and Thorne [1973] and Abel and Thorne [1998]. The processes are primarily ones of pitch angle transport, coulomb drag (energy transport), and atmospheric losses in competition with radial transport. Inside the plasmasphere, we expected the decay rates to be relatively constant. The difference between the initial decay rates in 1998–1999 and those in 2000–2001 may be caused by different levels of average magnetic activity and Hiss production for those periods. This will be examined in a later report.

Determining exactly how these processes combine to maintain the flux ratios will be a great challenge and will require a set of well designed missions that make the appropriate measurements over a range of equatorial L values, at least L = 2–6, simultaneous with measurements of electron precipitation at ionospheric altitudes. Hopefully, those missions are the NASA LWS Geospace Storms Investigations [*Kintner et al.*, 2002]

This page intentionally blank.

References

Abel, R. W. and R. M. Thorne, Electron scattering loss in Earth's inner magnetosphere, 1: Dominant physical processes, *J. Geophys. Res*., **103**, 2385, 1998

Baker, D., J. Blake, L. Callis, J. Cummings, D. Hovestadt, S. Kanekal, B. Klecker, R. Mewaldt, and R. Zwickl, Relativistic electron acceleration and decay time scales in the inner and outer radiation Belts: SAMPEX, *Geophys. Res. Lett.,* **21**, 409, 1994.

Blake, J. B., D. N. Baker, N. Turner, K. W. Ogilvie, and R. Lepping, Correlation of changes in the outer-zone relativistic-electron population with upstream solar wind and magnetic field measurements, *Geophys. Res. Lett.,* **24**, 927, 1997.

Blake, J. B., W. Kolasinski, R. Fillius, and E. Mullen, Injection of electrons and protons with energies of tens of MeV into L < 3 on 24 March 1991, *Geophys. Res. Lett,* **19**, 821, 1992.

Evans, M., N. Hastings, and B. Peacock, *Statistical distributions*, 3rd Ed., John Wiley and Sons, Inc., New York, N.Y., 2000.

Kanekal, S., D. Baker, and J. Blake, Multisatellite measurements of relativistic electrons: Global coherence, *J. Geophys. Res.,* **106**, 29721, 2001 (2001JA000070)

Kanekal, S., D. Baker, J. Blake, B. Klecker, R. Mewaldt, and G. Mason, Magnetospheric response to magnetic cloud (coronal mass ejection) events: Relativistic electron observations from SAMPEX and Polar, *J. Geophys. Res*, **104**, 24885, 1999 (1999JA900239)

Kintner, et al., The LWS Geospace Storm Investigations: Exploring the Extremes of Space Weather, NASA/TM-2002-211613.

Li, X., I. Roth, M. Temerin, J. Wygant, M. K. Hudson, and J. B. Blake, Simulation of the prompt energization and transport of radiation particles during the March 23, 1991 SSC, *Geophys. Res. Lett.,* **20**, 2423, 1993.

Lorentzen, K. R., J. B. Blake, U. S. Inan, and J. Bortnik, Observations of relativistic electron microbursts in association with VLF chorus, *J. Geophys. Res*, **106**, 6017, 2001a (2000JA003018).

Lorentzen, K. R., M. D. Looper, and J. B. Blake, Relativistic electron microbursts during the GEM storms, *Geophys. Res. Lett.,* **28**, 2573, 2001b (2001GL012926).

Lyons, L. R. and R. M. Thorne, Equilibrium structure of radiation belt electrons, *J. Geophys. Res,* **78**, 2142, 1973.

O'Brien, T. P., M. B. Moldwin, Empirical plasmapause models from magnetic indices, *Geophys. Res. Lett.,* **30**, 1152, 2003.

O'Brien, T. P., K. R. Lorentzen, I. R. Mann, N. P. Meredith, J. B. Blake, J. F. Fennell, M. D. Looper, D. K. Milling, and R. R. Anderson, Energization of relativistic electrons in the presence of ULF power and MeV microbursts: Evidence for dual ULF and VLF acceleration, *J. Geophys. Res.,* **108***,* 1329, 2003.

Olson, W. P., K. A. Pfitzer, and G. J. Mroz, Modeling the magnetospheric magnetic field, in Quantitative Modeling of Magnetospheric Processes, W. P. Olson ed., Am. Geophysical Union, 77, 1979

Tsyganenko, N. A., Quantitative models of the magnetospheric magnetic field: Methods and results, *Space Sci. rev.,* **54**, 1 1996.

Tsyganenko, N. A., Effects of the solar wind conditions on the global magnetospheric configuration as deduced from data-based field models, Eur. Space Agency Spec. Publ., ESA SP-389, 181, 1996.

LABORATORY OPERATIONS

The Aerospace Corporation functions as an "architect-engineer" for national security programs, specializing in advanced military space systems. The Corporation's Laboratory Operations supports the effective and timely development and operation of national security systems through scientific research and the application of advanced technology. Vital to the success of the Corporation is the technical staff's wide-ranging expertise and its ability to stay abreast of new technological developments and program support issues associated with rapidly evolving space systems. Contributing capabilities are provided by these individual organizations:

Electronics and Photonics Laboratory: Microelectronics, VLSI reliability, failure analysis, solid-state device physics, compound semiconductors, radiation effects, infrared and CCD detector devices, data storage and display technologies; lasers and electro-optics, solid-state laser design, micro-optics, optical communications, and fiber-optic sensors; atomic frequency standards, applied laser spectroscopy, laser chemistry, atmospheric propagation and beam control, LIDAR/LADAR remote sensing; solar cell and array testing and evaluation, battery electrochemistry, battery testing and evaluation.

Space Materials Laboratory: Evaluation and characterizations of new materials and processing techniques: metals, alloys, ceramics, polymers, thin films, and composites; development of advanced deposition processes; nondestructive evaluation, component failure analysis and reliability; structural mechanics, fracture mechanics, and stress corrosion; analysis and evaluation of materials at cryogenic and elevated temperatures; launch vehicle fluid mechanics, heat transfer and flight dynamics; aerothermodynamics; chemical and electric propulsion; environmental chemistry; combustion processes; space environment effects on materials, hardening and vulnerability assessment; contamination, thermal and structural control; lubrication and surface phenomena. Microelectromechanical systems (MEMS) for space applications; laser micromachining; laser-surface physical and chemical interactions; micropropulsion; micro- and nanosatellite mission analysis; intelligent microinstruments for monitoring space and launch system environments.

Space Science Applications Laboratory: Magnetospheric, auroral and cosmic-ray physics, wave-particle interactions, magnetospheric plasma waves; atmospheric and ionospheric physics, density and composition of the upper atmosphere, remote sensing using atmospheric radiation; solar physics, infrared astronomy, infrared signature analysis; infrared surveillance, imaging and remote sensing; multispectral and hyperspectral sensor development; data analysis and algorithm development; applications of multispectral and hyperspectral imagery to defense, civil space, commercial, and environmental missions; effects of solar activity, magnetic storms and nuclear explosions on the Earth's atmosphere, ionosphere and magnetosphere; effects of electromagnetic and particulate radiations on space systems; space instrumentation, design, fabrication and test; environmental chemistry, trace detection; atmospheric chemical reactions, atmospheric optics, light scattering, state-specific chemical reactions, and radiative signatures of missile plumes.